

1 **Identification of repurposable cytoprotective drugs for Vanishing White Matter Disease**

2 Neville Ng^{1,2}, Mauricio Castro Cabral-da-Silva^{1,2}, Simon Maksour^{1,3}, Tracey Berg^{1,2}, Martin
3 Engel^{1,2}, Dina M. Silva^{1,2}, Dzung Do-Ha^{1,2}, Jeremy S. Lum^{1,2}, Sonia Sanz Muñoz^{1,2}, Nadia
4 Suarez-Bosche^{1,2}, Claire H. Stevens^{1,2}, Lezanne Ooi^{1,2,*}

5 ¹Illawarra Health and Medical Research Institute, Wollongong, New South Wales, Australia

6 ²School of Chemistry and Molecular Bioscience and Molecular Horizons, University of
7 Wollongong, New South Wales, Australia

8 ³School of Medicine, University of Wollongong, New South Wales, Australia

9

10 **Corresponding Author:**

11 Dr Lezanne Ooi, Illawarra Health and Medical Research Institute, Building 32, University of
12 Wollongong, Wollongong, NSW 2522, Australia, Phone: +61 2 4298 5865, Email:
13 lezanne@uow.edu.au

14

15

16

17

18

19 Running title: VWMD drug repurposing screen

20 **Keywords:**

21 Vanishing white matter disease; leukodystrophy; cell stress; drug repurposing; induced
22 pluripotent stem cells; astrocytes

23

24 **Abstract**

25 Vanishing white matter disease (VWMD) is a rare leukodystrophy involving loss of function
26 mutations of the guanine exchange factor eIF2B and typically presenting with juvenile onset.
27 We aimed to identify repurposable FDA approved drugs in an *in vitro* drug screen using
28 patient-derived fibroblasts and induced pluripotent stem cell (iPSC)-derived astrocytes.
29 Dysregulated GADD34 and CHOP were identified in patient fibroblasts and iPSC-derived
30 astrocytes under proteasomal stress conditions. A drug screen from a 2400 FDA approved drug
31 library with *EIF2B5* disease patient fibroblasts identified 113 anti-inflammatory drugs as a
32 major class of hits with cytoprotective effects. A panel of potential candidate drugs including
33 berberine, deflazacort, ursodiol, zileuton, guanabenz and Anavex 2-73, and preclinical ISRIB,
34 increased cell survival of MG132-stressed *EIF2B2* and *EIF2B5* disease VWMD astrocytes,
35 and were further investigated for their effect on the integrated stress response and
36 mitochondrial stress. ISRIB but not other drugs significantly affected eIF2 α phosphorylation
37 and GADD34 expression. Ursodiol demonstrated capacity to reduce complex I subunit
38 upregulation, ameliorate oxidative stress, loss of mitochondrial membrane potential and
39 upregulation of eIF2B subunits in VWMD astrocytes, highlighting its potential as a
40 cytoprotective compound for VWMD.

41

42

43 **Introduction**

44 Vanishing white matter disease (VWMD) is a rare, autosomal recessive leukodystrophy,
45 caused by mutations in the genes, *EIF2B1*, *EIF2B2*, *EIF2B3*, *EIF2B4*, *EIF2B5*, encoding the
46 eukaryotic initiation factor eIF2B (1). The eIF2B protein is a guanine nucleotide exchange
47 factor that is involved in the integrated stress response (ISR) and loss of function mutations in
48 both alleles of an *EIF2B* gene leads to VWMD. VWMD is a debilitating and progressive
49 disease; patients are often diagnosed as children and survive few years beyond diagnosis.
50 Known mutations of *EIF2B* are considered to cause loss of function of the wild-type protein,
51 with variable onset, progression and severity, dependent on the precise mutations and
52 environmental stress factors (2).

53 The eIF2B proteins regulate mRNA translation, converting the inactive eIF2-GDP to the active
54 eIF2-GTP form (3). Activation the cytoprotective ISR leads to phosphorylation of eIF2 α (p-
55 eIF2 α), binding to eIF2B, translational repression, and upregulation of stress-induced genes
56 (4). These include GADD34, which facilitates dephosphorylation of p-eIF2 α toward recovery
57 from stress and resumption of normal protein translation in a negative feedback loop, and
58 transcription factors ATF4 and CHOP (5). The partial loss of function of eIF2B can lead to
59 delayed translation of stress-induced genes and dysregulated ISR expression (2). Although
60 eIF2B is ubiquitously expressed and plays a role in multiple cell types, the disease manifests
61 most significantly in the loss of white matter of the brain (6).

62 *EIF2B* mutant mouse models and induced pluripotent stem cell (iPSC) models (7, 8) have
63 identified a central role for dysfunctional astrocytes in the development of VWMD with
64 evidence for astrocytic apoptosis (8) and an inability to promote oligodendrocyte maturation
65 (6). A key driver of cellular pathogenesis in VWMD involves the ISR, with alterations in
66 responses to endoplasmic reticulum stress, proteasomal stress and oxidative stress (3).

67 Mitochondrial dysfunction and upregulated reactive oxygen species have been identified to be
68 upregulated in *EIF2B5*^{R132H/R132H} murine fibroblasts and astrocytes (9). Currently there are no
69 approved treatments for VWMD, hence the aim of this research was to identify candidate drugs
70 from an FDA approved drug library that could protect VWMD patient cells against cellular
71 stressors relevant to the disease.

72

73

74 **Results and Discussion**

75 **VWMD patient fibroblasts and astrocytes exhibit dysregulated ISR marker expression**

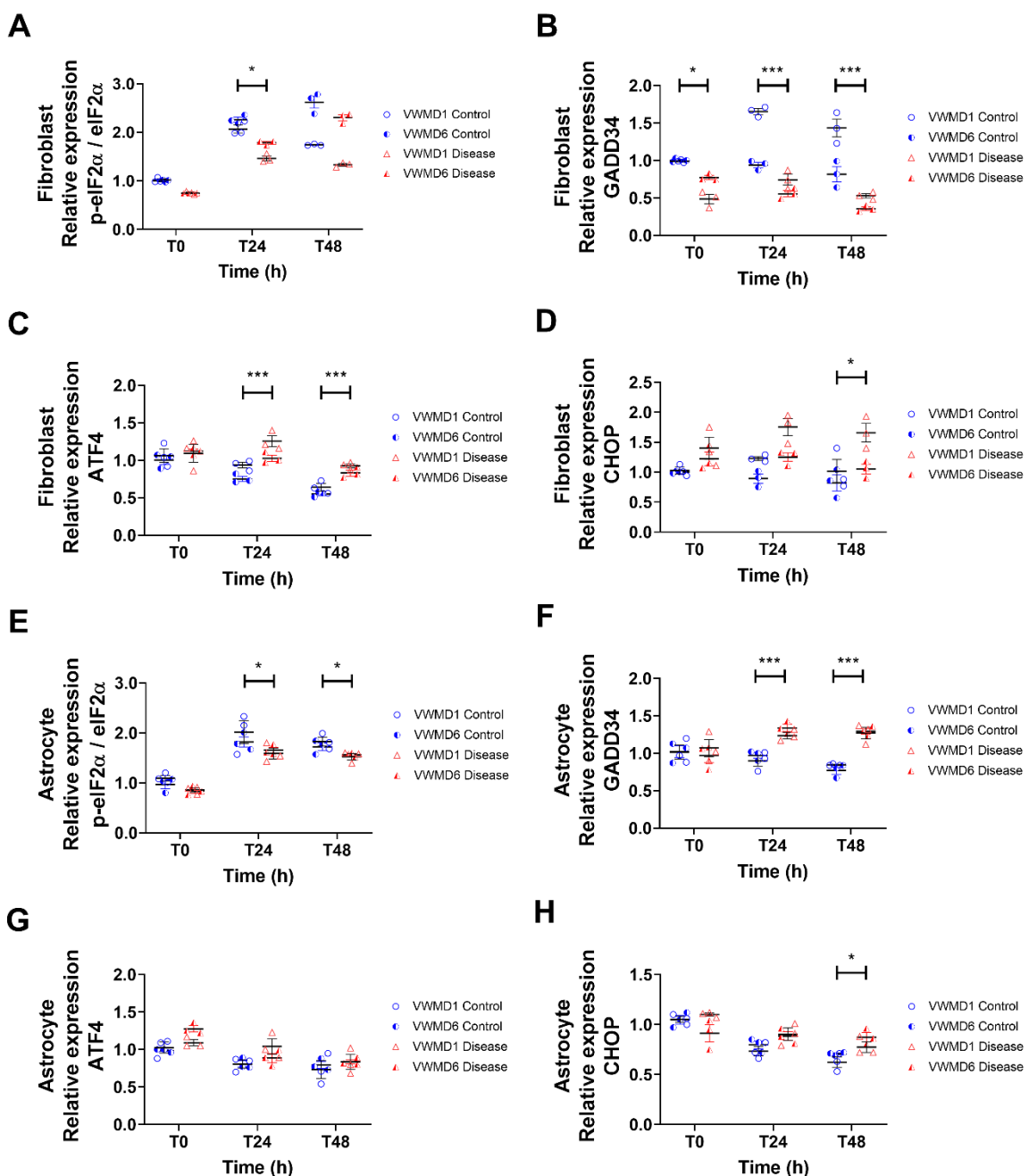
76 The partial loss of function of eIF2B has been observed to suppress both global and stress-
77 induced protein translation, in response to ER stress in VWMD patient lymphoblasts (2, 10).
78 Given that eIF2B is a ubiquitously expressed protein we anticipated that a dysfunctional ISR
79 may be evident in patient fibroblasts and iPSC-derived astrocytes. Fibroblasts were
80 reprogrammed into iPSCs from two VWMD patients, along with gender-matched relatives as
81 non-disease controls (Figure S1). The VWMD1 iPSC line was generated from a patient bearing
82 mutations in the *EIF2B5* gene (encoding eIF2B ϵ ^{R133H/A403V}), whilst the VWMD6 iPSC line was
83 generated from a patient bearing mutations in the *EIF2B2* gene (encoding eIF2B β ^{G200V/E213G}).
84 A previous study identified that white matter-derived astrocytes, generated using a CNTF-
85 based differentiation protocol, showed a more vulnerable phenotype to stress, compared to grey
86 matter astrocytes generated using FBS (7). Consequently, we generated astrocytes from iPSCs
87 using a CNTF-based method (Figure S2).

88 Responses to oxidative, proteasomal and endoplasmic reticulum (ER) stresses are all proposed
89 to be affected in VWMD cell and animal-based models (2, 11). Thus, we evaluated the dose-
90 dependent effect of H₂O₂, MG132 and thapsigargin stressors, as mediators of oxidative,
91 proteasomal and ER stress, respectively (Figure S3). There was a significant reduction in cell
92 survival for VWMD fibroblasts and iPSC-derived astrocytes, compared to non-disease
93 controls, under all three stressors (Figure S3).

94 MG132 is commonly utilised as a proteasomal inhibitor that can also induce ER and oxidative
95 stress via the unfolded protein response, all of which trigger the ISR (12). A key consequence
96 of partial loss of eIF2B function is disruption of ISR homeostasis, which can be assessed by
97 measuring the expression levels of ISR-relevant markers. The control of eIF2 α phosphorylation

98 or dephosphorylation acts as a pivotal mechanism that regulates global protein synthesis in
99 response to cell stress, as part of the ISR (13); GADD34 dephosphorylates eIF2 α (14). The
100 transcription factor ATF4 is an activator of the ISR in response to stress, while CHOP is
101 activated by the ISR to promote apoptosis (15). The expression levels of these four ISR-
102 relevant proteins, p-eIF2 α (normalised to eIF2 α), GADD34, ATF4 and CHOP, were compared
103 in VWMD and control fibroblasts and iPSC-derived astrocytes under MG132 stress (Figure 1).
104 Under proteasomal stress, VWMD and control fibroblasts exhibited similar decreases in eIF2 α
105 phosphorylation and GADD34 expression (Figure 1A-D), consistent with VWMD
106 lymphoblasts (2). However, elevated levels of ATF4 and CHOP were observed in MG132-
107 stressed VWMD fibroblasts, compared to controls, suggesting increased activation of the ISR.
108 MG132-stressed VWMD fibroblasts and astrocytes also exhibited increased CHOP, while
109 astrocytes exhibited increased GADD34 (Figure 1E-H), consistent with glia in animal model
110 studies (10).

111



112

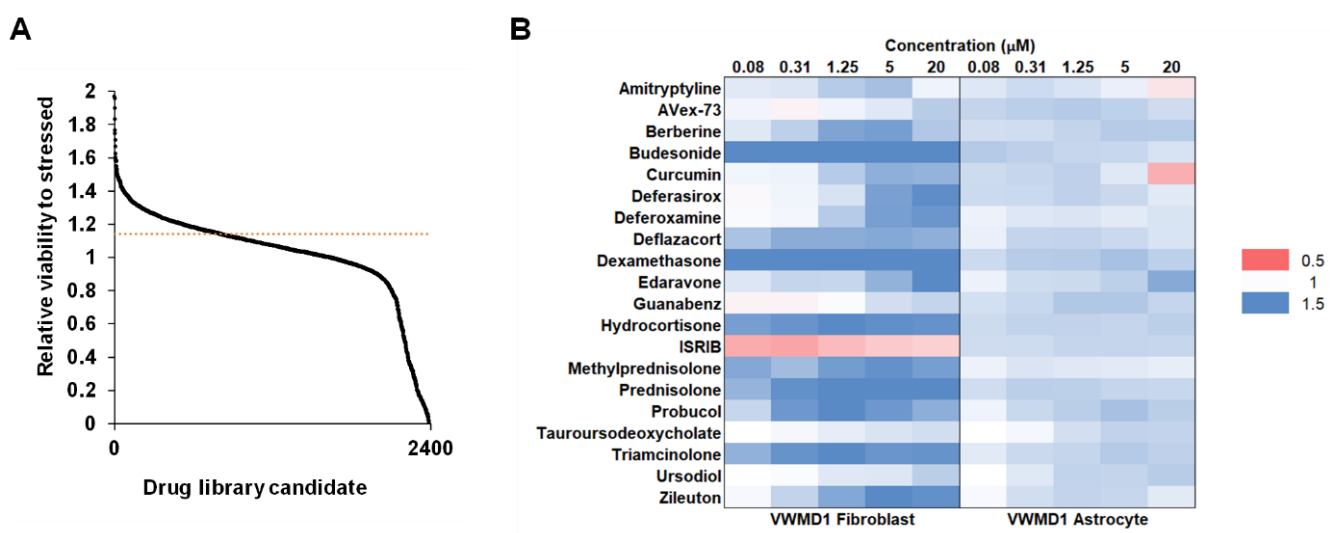
113 **Figure 1. ISR marker protein expression is affected in VWMD disease fibroblasts and astrocytes. (A-H)**
114 **Effect of MG132 stress on protein expression of the ISR markers, p-eIF2 α (normalised to eIF2 α), GADD34,**
115 **ATF4 or CHOP, at 0, 24 or 48 h incubation period. Protein levels were quantified by western blot,**
116 **normalised to total protein, and are shown relative to control at time 0. Individual data points are shown**
117 **from VWMD1 patient EIF2B5^{R133H/A403V} (open red triangle); VWMD6 patient EIF2B2^{G200V/E213G} (closed red**
118 **triangle) or their non-disease controls VWMD1 Control EIF2B5^{wt/wt}; VWMD6 Control EIF2B2^{G200V/wt} with**
119 **mean \pm SEM, n = 3. Significant differences were identified by two-way ANOVA followed by Holm-Sidak**
120 **posthoc test, * p < 0.05, ** p < 0.01, *** p < 0.001. Representative blots shown in (Figure S3).**

121

122

123 **Cytoprotective drug screen in VWMD patient lines**

124 Based on the established capacity of the proteasomal inhibitor, MG132, to induce proteasomal
125 stress, oxidative stress, and exacerbate ISR disease phenotypes, we performed a first-pass drug
126 screen for candidates able to protect against the effect of MG132 in VWMD1
127 *EIF2B5*^{R133H/A403V} patient fibroblasts, with cell viability assessed by resazurin reduction
128 activity (Figure 2).



129

130 Figure 2. Drug screen of cytoprotective candidates. (A) VWMD1 *EIF2B5*^{R133H/A403V} disease fibroblasts were
131 coincubated with MG132 and each of 2400 drugs from an FDA-approved drug library. Cell viability was
132 measured and normalised to cell viability with MG132 stressor in the absence of drug. Drugs were ranked
133 based on increase in cell viability (n = 3). Cytoprotection ranged from 2-fold increase in viability to 0 (100%
134 cell death for cytotoxic drugs). Horizontal dotted red line indicates 1.5 x standard deviation of MG132
135 stressed controls. (B) Hit candidates were taken forward to assess their dose response effect on cell viability
136 of VWMD1 *EIF2B5*^{R133H/A403V} fibroblasts and iPSC-derived astrocytes, relative to MG132 stress (n = 5-6).
137 ISRB was included due to its previous identification as a potential treatment for VWMD, although it
138 caused significant toxicity in fibroblasts. Heat map represents cytoprotection (blue) versus cytotoxicity
139 (red) of individual drugs.

140

141 Following the initial drug screen, a panel of 20 compounds (Table S2) was selected for
142 downstream evaluation in VWMD1 *EIF2B5*^{R133H/A403V} fibroblasts and in both VWMD1
143 *EIF2B5*^{R133H/A403V} and VWMD6 *EIF2B2*^{G200V/E213G} patient-derived astrocyte lines. The
144 compounds selected for downstream assays were chosen based on their translational premise,
145 including considerations of bioavailability, route of administration and complications in
146 treatment. The drug panel included 15 protective compounds from the screen (>1.5 x standard

147 deviation of MG132-stressed controls), and a further five compounds with relevant modes of
148 action for VWMD. Overall, this panel included glucocorticosteroids, bile acids, iron chelators,
149 antioxidants, ISR modulators and sigma-1 receptor agonists. Nominated drugs included
150 guanabenz, ISRIB, sigma-1 receptor agonists, AVex-73 and amitriptyline,
151 taurooursodeoccyholic acid and alkaloid berberine. All candidates elicited cytoprotective effects
152 against MG132-induced stress at varying concentrations in VWMD1 fibroblasts, with the
153 exception of ISRIB. Ursodiol and its taurine derivative, taurooursodeoxycholic acid, showed
154 similar cytoprotective efficacies. We observed that anti-inflammatories were amongst the
155 largest category of compounds that improved cell viability under proteasomal stress, with a
156 high proportion of these being glucocorticosteroids. Steroids can regulate inflammation,
157 mitochondrial function and apoptosis toward neuroprotective effect in brain injury,
158 Alzheimer's disease, Parkinson's disease, multiple sclerosis, and stroke (16). Although
159 glucocorticosteroids are a commonly administered class of drugs, an anecdotal study of
160 corticosteroids on three VWMD patients did not identify benefits and the patients were
161 removed from this treatment due to potential clinical complications (17). Deflazacort was
162 selected as a representative glucocorticosteroid on the basis of fewer reports of adverse effects
163 in the literature and its use in the clinic, including in children with muscular dystrophy (18, 19).
164 The recent demonstration of mitochondrial dysfunction and inefficient respiration in murine
165 models of VWMD (9) has expanded the search for possible therapeutics to include
166 mitochondrial protective compounds and antioxidants (3, 9). The protective effect of the
167 antioxidant edaravone was evident in astrocytes at a higher efficacy than any other candidate,
168 potentially due to its well established radical scavenging activity (20). Edaravone was recently
169 approved for amyotrophic lateral sclerosis and while its administration is currently limited to
170 intravenous injection, oral and mucosal formulations are in development (21-23). The sigma-
171 1 receptor is a chaperone protein in ER membranes that governs a range of cellular processes,

172 including calcium homeostasis and reactive oxygen species accumulation (11). However, in
173 this study, the cytoprotective effect of the sigma-1 receptor agonists, AVex-73 and
174 amitriptyline, was limited at higher concentrations ($\geq 5 \mu\text{M}$).

175 VWMD6 *EIF2B2*^{G200V/E213G} iPSC-derived astrocytes confirmed the findings in VWMD1
176 *EIF2B5*^{R133H/A403V} iPSC-derived astrocytes (Figure S4). Of those tested, the majority of the
177 drugs that were protective in VWMD1 fibroblasts were also protective in VWMD1 and
178 VMWD6 astrocytes, with the exception of amitriptyline, curcumin and budesonide (Figures 2,
179 S4).

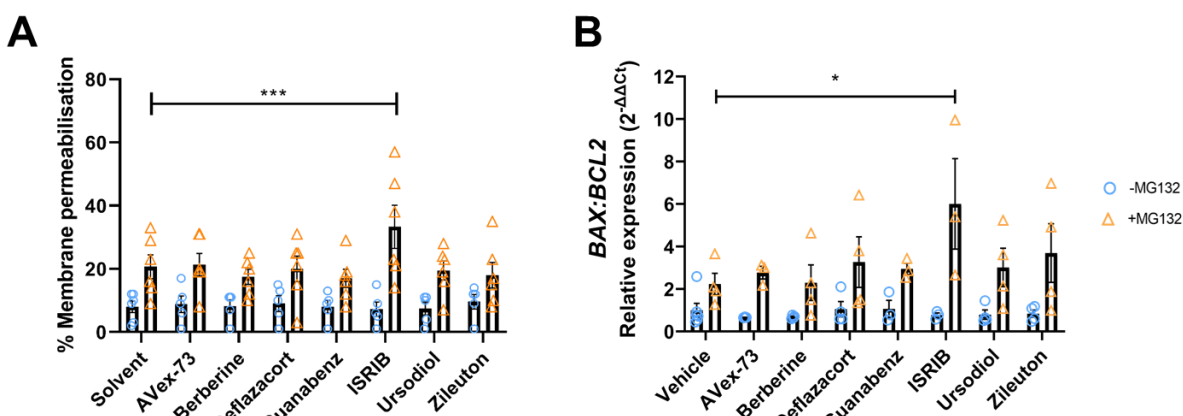
180

181 **Effect of candidate drugs on mode of cell death**

182 We further investigated the effects of a panel of compounds, in order to provide insight into
183 potential modes of cytoprotective action. For these experiments we assessed drugs with strong
184 translational potential for VWMD (Figures 2, S4), including Avex-73, berberine, deflazacort,
185 guanabenz, ISRib, ursodiol and zileuton. We did not include edaravone, despite its promising
186 effects in patient fibroblasts and astrocytes, due to its intravenous route of administration.

187 Assays to investigate potential drug mechanisms were performed using MG132 stress-induced
188 VWMD1 *EIF2B5*^{R133H/A403V} patient astrocytes, as the most common VWMD subunit mutation
189 (24). To determine whether candidate drugs reduced the proportion of bulk cell death, the
190 membrane permeabilisation of treated astrocyte cultures was evaluated. In MG132-stressed
191 VWMD1 astrocytes there were no significant changes in the percentage of membrane-
192 permeabilised cells, with the exception of ISRib increasing the proportion of membrane-
193 permeabilised cells (Figure 3A). To test whether the drugs caused a reduction in mitochondrial
194 apoptosis, the *BAX:BCL2* ratio was evaluated. There was no detectable change in *BAX:BCL2*
195 ratio caused by any of the drug candidates, with the exception of an increase in *BAX:BCL2*

196 caused by ISRIB (Figure 3B). Together these data show that astrocytes coincubated with
197 MG132 and ISRIB exhibited an overall increase in cell viability, despite having an elevated
198 proportion of membrane-permeabilised cells and increased *BAX:BCL2* ratio. This apparent
199 paradox may reflect the ability of ISRIB to promote protein synthesis under stress conditions,
200 and thus support a greater turnover of the cell population. ISRIB may thus have an adverse
201 effect on cell survival under acute stress conditions, particularly for non-cycling cells, such as
202 neurons. The ramifications of this are yet to be reported in animal studies (25, 26), however
203 the enhanced effect of cytotoxic drugs under an ISRIB-suppressed ISR have been recently
204 demonstrated in prostate and pancreatic cancer studies (27, 28). Further testing of ISRIB in
205 animal studies will uncover details of its precise role on cell survival during different stress
206 conditions.

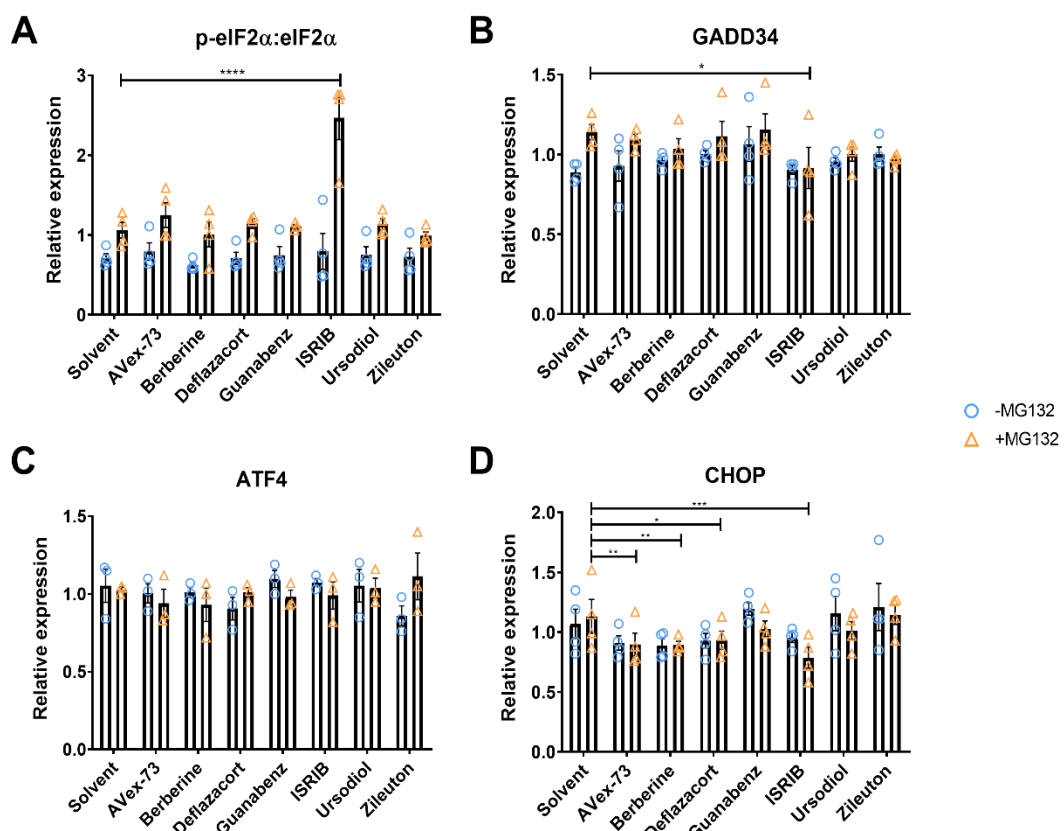


207
208 **Figure 3. Effect of candidate drugs on membrane permeabilisation and mitochondrial pathway cell death**
209 **markers in vehicle control (blue circle) or 0.1 μ M MG132-treated (orange triangle) VWMD1**
210 ***EIF2B5*^{R133H/A403V} patient iPSC-derived astrocytes.** Cells were treated with candidate drugs, with or
211 without MG132 for 24 h. (A) Ethidium homodimer was used to quantify % membrane permeabilised
212 astrocytes (n = 5-6). (B) RT-qPCR was used to measure gene expression changes of the mitochondrial
213 apoptosis pathway indicator, *BAX:BCL2* ratio (n = 3-4). Individual data points are shown with mean \pm
214 SEM; significant differences are shown by * p < 0.05, *** p < 0.001, identified by two-way ANOVA
215 followed by Holm-Sidak posthoc test.

216

217 **Effect of candidate drugs on ISR-relevant proteins, p-eIF2 α , GADD34, ATF4 and CHOP**

218 A key consequence of partial loss of eIF2B function is disruption of ISR homeostasis, thus
219 candidate drugs were assessed for their effect on the ISR under MG132 stress. The expression
220 levels of the ISR-relevant proteins, p-eIF2 α (normalised to eIF2 α), GADD34, ATF4 and
221 CHOP, were evaluated following candidate drug treatment (Figure 4A-D). ISRB markedly
222 increased p-eIF2 α and decreased GADD34 and CHOP expression under MG132 stress
223 conditions (Figure 4A-D). No significant changes in ATF4 were detected by any of the drugs
224 (Figure 4C). However, AVex-73, berberine and deflazacort significantly decreased CHOP
225 expression in the presence of MG132 (Figure 4D).



226

227 **Figure 4. Effect of candidate drugs on ISR markers in vehicle control (blue circle) or 0.1 μ M MG132-
228 treated (orange triangle) VWMD1 EIF2B5^{R133H/A403V} patient iPSC-derived astrocytes. Cells were treated
229 with candidate drugs, with or without MG132 for 24 h. Protein expression was measured by western blot
230 and normalised to total protein for the ISR markers: (A) phosphorylated eIF2 α , normalised to eIF2 α ; (B)
231 GADD34; (C) ATF4; (D) CHOP. Individual data points are shown with mean \pm SEM (n=4). Significant**

232 **differences were identified by two-way ANOVA, followed by Holm-Sidak posthoc test * p < 0.05, ** p <**
233 **0.01, *** p < 0.001, **** p < 0.0001. Representative western blots shown in (Figure S6).**

234
235 Previous cell stress and neurodegeneration studies have established ISR-modulating roles for
236 guanabenz and ISRib (29, 30), hence their inclusion in our panel of compounds. Guanabenz is
237 considered to exert cytoprotective effects by inhibiting the activity of GADD34 to recruit eIF2
238 phosphatases, thus prolonging translation inhibition and avoiding the stress of resuming protein
239 synthesis (29). However, at concentrations of guanabenz that induced a cytoprotective effect
240 (5 μ M) we did not observe a significant impact on expression of any ISR markers. Conversely,
241 ISRib-mediated cytoprotection of astrocytes (1.25 μ M) was associated with increased eIF2 α
242 phosphorylation, and downregulation of GADD34 and CHOP.

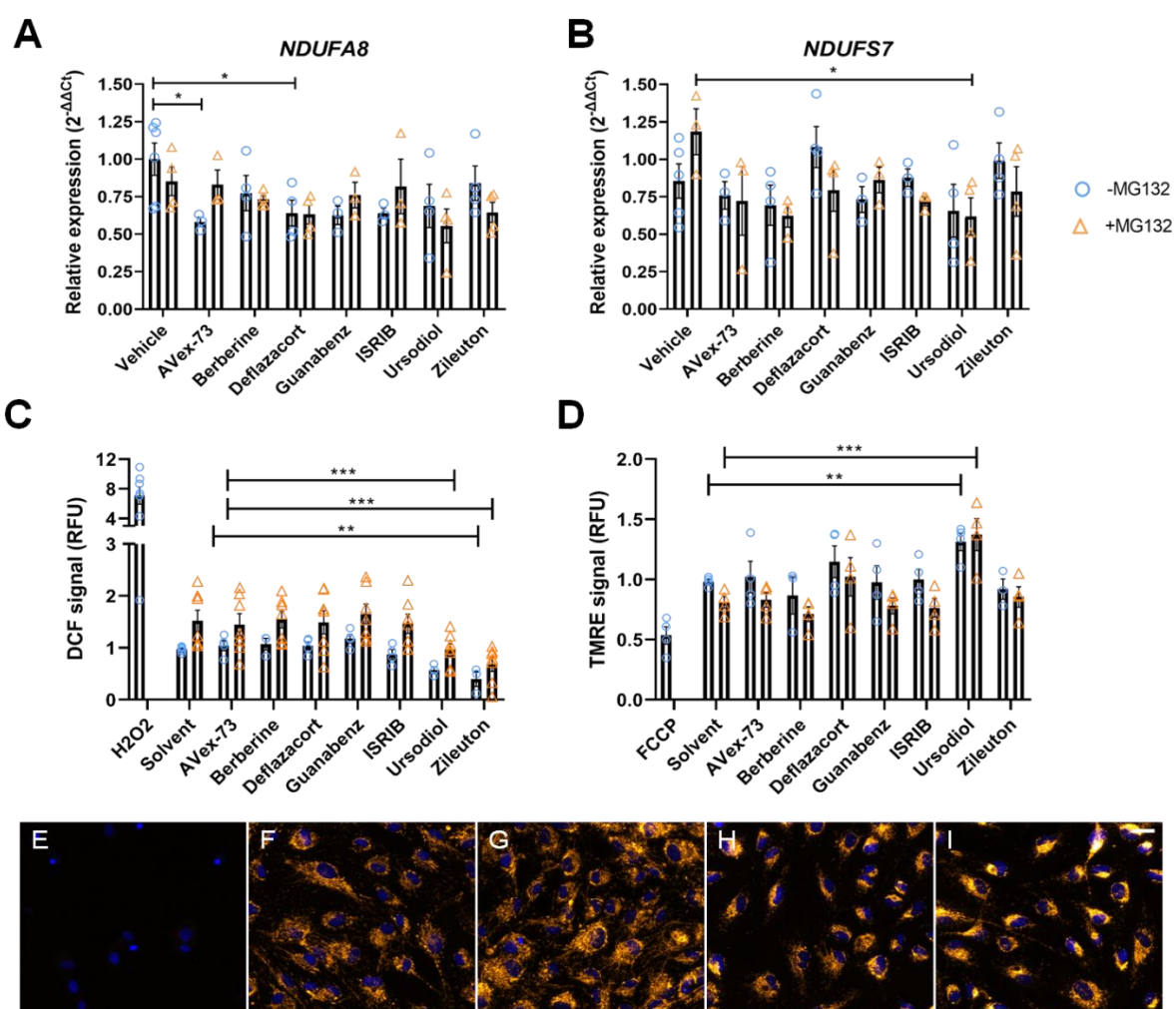
243 ISRib is thought to allow eIF2B to escape inhibitory complex formation with p-eIF2 α , in order
244 to limit repression of protein synthesis while under ER stress (10, 31). An analogue of ISRib
245 was recently shown to improve ISR signature, motor function and myelin loss in a *EIF2B5*
246 VWMD mouse model (10, 31). However, in this study, ISRib exacerbated MG132 toxicity in
247 *EIF2B5* VWMD fibroblasts at all doses (0.08-20 μ M), consistent with prior reports that ISRib
248 enhances thapsigargin-induced apoptosis in HEK293T cells (26). It is also worth noting that
249 the stabilising effect of ISRib may be mutation-dependent (3). The phytochemical, berberine,
250 was included in the panel because it is considered to be a well-tolerated natural compound (32).
251 In MG132-stressed astrocytes berberine treatment increased cell viability, potentially via
252 decreasing pro-apoptotic CHOP (Figure 4D). The antioxidant, anti-inflammatory, ER and
253 mitochondrial protective effects of berberine have been noted in numerous studies, including
254 increased levels of antioxidants, superoxide dismutase and glutathione, inhibition of caspase 3
255 activity and apoptosis and decreased cytochrome C and *BAX:BCL2* ratio in ischemic injury and
256 diabetic animal models (33, 34).

257 **Effect of candidate drugs on indicators of mitochondrial function**

258 The eIF2B mutations in murine models have been shown to affect mitochondrial complex I
259 function and increase mitochondrial abundance (35). To identify potential mitochondrial
260 protective mechanisms, we assessed the effect of the candidate drugs on the expression levels
261 of mitochondrial complex I using the markers, *NDUFA8* and *NDUFS7*, in VWMD1
262 *EIF2B5*^{R133H/A403V} astrocytes. Ursodiol significantly prevented complex I subunit increases in
263 *NDUFS7* caused by MG132, while AVex-73 and deflazacort reduced *NDUFA8* expression
264 (Figure 5A-B). A reduction in complex I subunit expression and CHOP expression may reflect
265 the ability of deflazacort to improve mitochondrial biogenesis (36). AVex-73 decreased
266 VWMD1 astrocyte expression of complex I subunit in the absence of stressor, which may
267 indicate a decrease in respiratory burden, although this was not evident under MG132 stress
268 (11). Mutations in eIF2B genes impair mitochondrial function during oxidative stress
269 conditions and suggest a dysregulated ISR in VWMD murine fibroblasts and astrocytes (9),
270 consistent with our findings.

271 The candidate drugs were further investigated for their effects on oxidative stress and
272 mitochondrial membrane potential. Ursodiol and zileuton significantly decreased DCF signal,
273 as an indicator of reactive oxygen species generation, in VWMD1 *EIF2B5*^{R133H/A403V} patient
274 astrocytes, in the presence or absence of MG132 stress (Figure 5C). Of the anti-inflammatory
275 candidate drugs, the 5-lipoxygenase antagonist zileuton, demonstrated significant reduction in
276 generation of reactive oxygen species, a finding that correlates with its radical scavenging
277 activity (37). Ursodiol also increased relative mitochondrial membrane potential of VWMD1
278 *EIF2B5*^{R133H/A403V} astrocytes under both unstressed and stressed conditions, based on the
279 TMRE assay (Figure 5D-I). Together, these data suggest that ursodiol may promote
280 mitochondrial function and reduce oxidative stress in VWMD astrocytes.

281



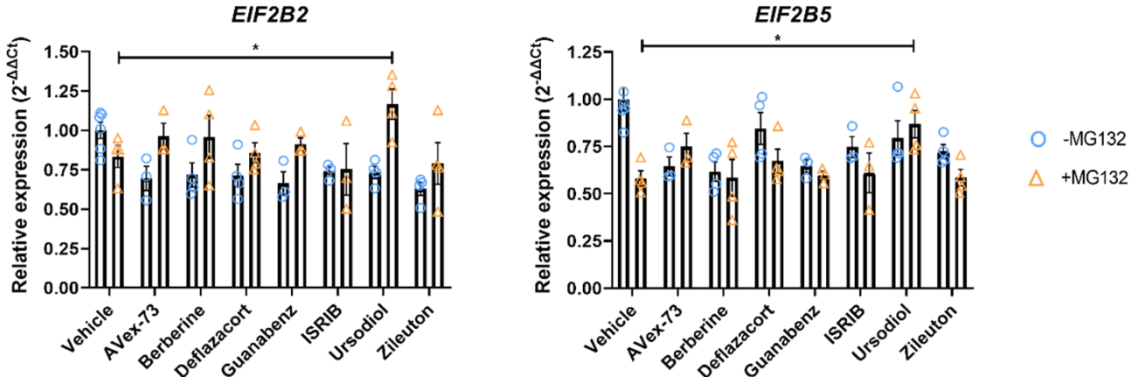
282

283 **Figure 5. Effect of candidate drugs on complex I subunit expression, oxidative stress and mitochondrial**
284 **membrane potential in VWMD1 *EIF2B5*^{R133H/A403V} disease astrocytes.** VWMD1 iPSC-derived astrocytes
285 were treated with vehicle control (DMSO; blue circle) or 0.1 μ M MG132 (orange triangle) and candidate
286 drugs for 24 h. Expression of mitochondrial complex I subunits was measured by RT-qPCR for (A)
287 *NDUFA8* and (B) *NDUFS7*. (C) Reactive oxygen species was measured via DCF fluorescence and (D)
288 TMRE fluorescence was used to measure mitochondrial membrane potential. Representative confocal
289 fluorescence microscopy images of: (E) FCCP (protonophore, mitochondrial uncoupler, loss of TMRE
290 fluorescence), (F) TMRE assay solvent, (G) ursodiol, (H) MG132, (I) MG132 + ursodiol (scale bar = 30 μ m)
291 (orange = TMRE; blue = Hoechst 33342 nuclear stain). For A-D individual data points are shown and mean
292 \pm SEM from replicate differentiations (n=4-6); significant differences were identified by two-way ANOVA
293 followed by Holm-Sidak posthoc test * p < 0.05, ** p < 0.01, *** p < 0.001.

294

295 Ursodiol rescues repression of *EIF2B2* and *EIF2B5* gene expression

296 The potential cytoprotective effect of candidate drugs, as a result of upregulation of *EIF2B*
297 genes, was considered. In MG132-stressed VWMD1 *EIF2B5*^{R133H/A403V} astrocytes, ursodiol
298 rescued reductions in *EIF2B2* and *EIF2B5* expression (Figure 6).



299

300 **Figure 6. Gene expression changes of *EIF2B2* and *EIF2B5* genes in VWMD1 *EIF2B5*^{R133H/A403V} patient**

301 astrocytes treated with vehicle control (DMSO; blue circle) or 0.1 μM MG132 (orange triangle) and

302 candidate drugs for 24 h. Relative expression was evaluated by RT-qPCR for: (A) *EIF2B2* and (B) *EIF2B5*.

303 Individual data points are shown with mean ± SEM, n=4. Significant differences were identified by

304 two-way ANOVA followed by Holm-Sidak posthoc test, * p < 0.05.

305

306 Together the data identified that one of the most promising drugs for clinical translation is

307 ursodiol, a bile acid naturally formed in the liver and administered for gallstones. Ursodiol has

308 demonstrated capacity to cross the blood brain barrier, based on clinical trials for motor

309 neurone disease, reaching levels in cerebral spinal fluid that, based on the findings here, could

310 be protective (38). Additionally, ursodiol has been identified as protective in other

311 neurodegenerative and optical atrophy research (39, 40). Anti-apoptotic and neuroprotective

312 effects of ursodiol were observed, though the underlying molecular mechanism of ursodiol-

313 mediated protection was not identified in these studies (39, 40). Progression of VWMD

314 includes glial cell death, developing towards neuronal cell death, and leading to paralysis and

315 neuropathy (41). We observed ursodiol to decrease oxidative stress and possibly mitochondrial

316 complex I burden, increase mitochondrial membrane potential, ameliorate stress-induced

317 decreases in *EIF2B* gene expression, and improve cell viability in VWMD astrocytes under

318 proteasomal stress. The increase of mitochondrial membrane potential by ursodiol identified

319 in our study has also been previously observed in Alzheimer's disease patient fibroblasts (42).

320 Considering disrupted mitochondrial function has been extensively implicated in VWMD and

321 a wide range of neurodegenerative disorders, further investigation of the neuroprotective
322 effects of ursodiol are warranted. The hypothetical premise of cytoprotective drugs are those
323 that can deliver increased cell viability, limiting disease-related degeneration. Together with
324 information from previous studies on other CNS diseases (38, 42) our preliminary findings are
325 supportive toward further investigation of ursodiol and anti-inflammatory drugs as
326 cytoprotective agents for VWMD.

327

328 **Methods**

329 **Cell culture**

330 All experimental protocols were approved by the University of Wollongong Human Research
331 Ethics Committee (HE17/522). Primary human dermal fibroblasts were collected from VWMD
332 patients (2) or control family members (2) and maintained in DMEM/F12 (Life Technologies,
333 21331020), 10% FBS (Bovogen, SFBS-AU), 2 mM L-glutamine (Life Technologies,
334 25030081) and 1% penicillin/streptomycin (Life Technologies, 15140122). The mRNA-based
335 reprogramming of patient fibroblasts into iPSCs, pluripotency marker immunofluorescence
336 and RT-qPCR, karyotyping and mutation genotype characterisation are described in
337 Supplementary Information (Figure S1). The iPSCs were maintained in mTESR1 (Stem Cell
338 Technologies, 85850). Astrocytes were maintained in Astrocyte Growth Supplement Medium
339 (AGS; Sciencell, 1852). All cells were maintained in humidified incubators at 37 °C
340 supplemented with 5% CO₂ for fibroblasts or hypoxic 3% O₂ conditions for iPSCs. Neural
341 inductions were carried out as previously described (43). Astrocyte differentiations were
342 performed in ciliary neurotrophic factor (CNTF), epidermal growth factor (EGF) and basic
343 fibroblast growth factor (FGF2)-based medium and transitioned to AGS, prior to
344 characterisation by immunofluorescence and inflammatory activation, to confirm the

345 production of functional astrocytes from iPSCs. Details of neural inductions and astrocyte
346 differentiations are in Supplementary Information (Figure S2).

347 **Cell viability assay**

348 Fibroblasts or astrocytes (5000 cells/well) were seeded in 96 well plates and incubated with a
349 range of concentrations of hydrogen peroxide (H₂O₂; 0-2000 μM), MG132 (0-20 μM; Focus
350 Bioscience, HY-13259) or thapsigargin (0-20 μM) overnight before incubation with 15 μM
351 resazurin for 1 h and acquisition by fluorescence plate spectroscopy (excitation 544 / emission
352 590). For coincubation assays, cells were similarly prepared and incubated with candidate
353 drugs and 2.5 μM MG132 (fibroblasts;) or 0.1 μM MG132 (astrocytes) for 48 h based on the
354 IC₆₀ for each cell type (Figure S3). Following incubation, cell viability was assessed by a
355 resazurin reduction assay (Life Technologies, A13262). The coincubation drug screen was
356 carried out in VWMD1 patient fibroblasts with the MicroSource Spectrum FDA collection
357 (Compounds Australia), a library of 2400 FDA-approved drugs. Cell seeding and drug reagent
358 preparation was performed by a robotic liquid handler (Hamilton Microlab Star). Single drug
359 concentrations were selected based on protective efficacy in dose response coincubation assays
360 and used in downstream assays at concentrations of: Annavex 2-73 (AVex-73, 5 μM),
361 berberine (1.25 μM), guanabenz (5 μM), ISRIB (1.25 μM), deflazacort (5 μM), ursodiol (40
362 μM) and zileuton (1.25 μM). All treatments were performed in technical duplicate wells.

363 **Integrated stress response protein quantification**

364 Fibroblasts or astrocytes were seeded in 6 well plates (200,000 cells/well) and incubated with
365 MG132 for 0, 24 or 48 h, or coincubated with candidate compound and MG132 overnight.
366 Cultures were lysed in RIPA buffer (50 mM Tris, pH 8.0, 150 mM NaCl, 1% Triton X-100,
367 0.5% Sodium Deoxycholate, 0.1% SDS and protease and phosphatase inhibitors) and stored at
368 -20°C before sonication and quantification by a Pierce BCA Protein Assay Kit (Thermofisher

369 Scientific, 23225). Protein lysates were heated for 5 min at 95°C in loading buffer (1% SDS,
370 5% 2-mercaptoethanol, 6.25% glycerol, 0.001% bromophenol blue, 0.030 M Tris-HCl, pH
371 6.8). Denatured protein lysates (5 µg) were loaded in 4–20% Criterion TGX Precast Gels (Bio-
372 Rad, 5678095) and transferred to Immobilon-FL PVDF membrane (0.45 µm pore; Merck,
373 IPFL00010). Membranes were incubated with 0.5% casein (Bio-rad, 1610782) for 1 h, primary
374 antibody for 16 h (4 °C), and secondary antibody at 1 h (4 °C) facilitated by an automated
375 western blot liquid handler (Cytoskeleton GOBlot). Antibodies utilised included anti-eIF2α
376 (abcam, ab5369), anti-eIF2α-phopsho-S51 (abcam, ab32157), anti-ATF-4 (abcam, ab23760),
377 anti-DDIT3 (abcam, ab179823), anti-GADD34 (abcam, ab126075), donkey anti-mouse Alexa
378 Fluor Plus 488 (Thermofisher Scientific A32766) and donkey anti-rabbit Alexa Fluor Plus 647
379 (Thermofisher Scientific A32795). All primary antibody dilutions were performed at 1:1000,
380 secondaries at 1:5000. Blots were imaged with a Bio-Rad ChemiDoc MP. Band intensities
381 were normalised to stain-free total protein. Relative eIF2α phosphorylation was normalised to
382 eIF2α. Dynamic range of signal was confirmed by linear signal to loading ratio (Figure S6).

383 **RT-qPCR cell stress assay**

384 Total RNA was harvested using the PureLink RNA Mini Kit (Life Technologies, 12183025)
385 as per manufacturer's instructions. RNA quality was assessed using the NanoDrop 2000
386 Spectrophotometer (Thermofisher Scientific) with A_{260/280} ratio from 1.9 to 2.1. Up to 1 µg of
387 RNA was used to synthesise cDNA using the iScript gDNA Clear cDNA Synthesis Kit (Bio-
388 Rad, 1725035) and PowerUp SYBR Green (Thermofisher Scientific, A25778) was used for
389 quantitative PCR. Primers were used at 400 nM (**Table 1**). Primer annealing temperatures were
390 optimised by a serial dilution standard curve and considered acceptable within a range of 85-
391 110% efficiency. RT-qPCR was performed using the QuantStudio 5 Real-Time PCR System
392 (Applied Biosystems). Each reaction was run in triplicate and contained 20 ng of cDNA
393 template in a final reaction volume of 20 µL. Cycling parameters were: 50 °C for 2 min, 95 °C

394 for 2 min, then 40 cycles of 95 °C for 1 s and the annealing/extending temperature for each
395 primer (**Table 1**) for 30 s, followed by conditions for melt curve analysis: 95 °C for 15 s, 60 °C
396 for 1 min and 95 °C for 15 s. ΔCt values were obtained by normalisation to the average of three
397 housekeeper genes, *GAPDH*, *HPRT* and *PPIA*. Data are presented using the $2^{-\Delta\Delta Ct}$ calculation
398 to yield relative gene expression values (fold change).

399 **Table 1. List of primers used for gene expression assay**

Target	Forward primer (5' – 3')	Reverse primer (5' – 3')	Annealing temperature (°C)	Supplier
<i>GAPDH</i>	GAGCACAAAGAGGAAGAG AGAGACCC	GTTGAGCACAGGGTACT TTATTGATGGTACATG	58	Sigma-Aldrich
<i>HPRT</i>	ATAAGCCAGACTTTGTTG G	ATAGGACTCCAGATGTT TCC	60	Sigma-Aldrich
<i>PPIA</i>	ACGTGGTATAAAAGGGG CGG	CTGCAAACAGCTAAA GGAGAC	60	Sigma-Aldrich
<i>BAX</i>	CCTTTCTACTTGCAG CAAAC	GAGGCCGTCCCAACCA C	60	Life Technologies
<i>BCL2</i>	GATTGTGGCCTCTTGA G	GTTCCACAAAGGCATCC	60	Sigma-Aldrich
<i>EIF2B1</i>	TATTGACTCACGCCACT CCA	GCATCTAGCACCAAGT GACA	60	Sigma-Aldrich
<i>EIF2B2</i>	GAGCTGCTAGTGGAGCT GG	GGCCTCTACTGTTGGGG AGAA	62	Sigma-Aldrich
<i>EIF2B3</i>	CCGGAGTGAAGTGATTCC AT	ATTCCAGCAGGCATCAT AGG	60	Sigma-Aldrich
<i>EIF2B4</i>	TCACCTACCCAGTACAG CA	CTGGGTGGATCACAGA GGAT	60	Sigma-Aldrich
<i>EIF2B5</i>	TTCTGGTGGCCGATAGCT TC	AGCTTCCAGCAACAAA AGACA	60	Sigma-Aldrich
<i>NDUFA8</i>	AAGGTACCAAAAGTGAA AAC	TTTTCATCAGTCGTTGT CTG	60	Sigma-Aldrich
<i>NDUFS7</i>	AAGGTCTACGACCAGAT G	CCACCGAGTGGAATAG TG	60	Sigma-Aldrich

400

401 **Oxidative stress and mitochondrial membrane potential microscopy assays**

402 Astrocytes (10,000 cells per well) were seeded in 96 well plates and coincubated overnight
403 with MG132, as described above, and candidate drugs, or the positive controls for oxidative
404 stress: H₂O₂ (100 μ M), or the proton uncoupler carbonyl cyanide-4-phenylhydrazone (FCCP;
405 10 μ M; Focus Bioscience, HY-100410-10MG). Cells were loaded with 20 μ M H2DCFDA
406 (DCF, Life Technologies, D399) or 0.5 μ M tetramethylrhodamine ethyl ester (TMRE, Life

407 Technologies, T669) and 10 μ M Hoescht 33342 (Sigma-Aldrich, B2261-25MG) for 0.5 h
408 before replacement of medium with phenol-red free medium and further incubation for 1 h.
409 Relative fold change in DCF signal was acquired by fluorescence spectroscopy and normalised
410 to cell density quantified by 0.04% sulforhodamine B (Sigma-Aldrich, 230162) solublised in
411 10 mM Trizma (Sigma-Aldrich, T1503) after fixation in 4% trichloroacetic acid (Sigma-
412 Aldrich, T9159) (44). TMRE images were acquired by confocal microscopy and analysed with
413 ImageJ to determine fluorescence normalised to cell density.

414 **Statistical analyses**

415 Data are presented as the mean and standard error of the mean of at least 3 independent
416 experiments, statistical significance was assessed by two-way analysis of variance followed by
417 Holm-Sidak posthoc test for multiple comparisons unless otherwise stated. Significance was
418 accepted where $p < 0.05$. Charts and statistical analyses were prepared in Prism GraphPad 8.0.

419

420 **Acknowledgements**

421 This research was funded by philanthropic donations and a grant from the Illawarra Health and
422 Medical Research Institute (IHMRI). L.O. is supported by a National Health and Medical
423 Research Council (NHMRC) of Australia Boosting Dementia Research Leadership Fellowship
424 (APP1135720). The authors thank Dr Gil Stynes (IHMRI, and Department of Surgery,
425 Wollongong Hospital) for fibroblast collection and Prof Justin Yerbury, A/Prof Mirella Dottori
426 and Prof Heath Ecroyd for valuable discussions, and Dr Reece Gately and Rachelle Balez for
427 technical assistance. The authors wish to thank all of the donors, the patients and their families
428 that have made this research possible.

429 **Author contributions**

430 NN – data generation, data analysis, manuscript writing; MC – data generation, data analysis;
431 TB – data generation, data analysis; SM – data generation, data analysis; ME - data generation;
432 DS - data generation; DDH – data analysis; JL – data generation; SSM – data analysis; NSB –
433 data generation; CS – data generation; LO - intellectual input, data analysis, manuscript
434 writing, supervision, funding. All authors reviewed the manuscript.

435 **Conflict of Interest**

436 The authors declare no conflict of interest.

437 **References**

- 438 1. Bugiani M, Vuong C, Breur M, van der Knaap MS. Vanishing white matter: a
439 leukodystrophy due to astrocytic dysfunction. 2018;28(3):408-21.
- 440 2. Moon SL, Parker R. EIF2B2 mutations in vanishing white matter disease hypersuppress
441 translation and delay recovery during the integrated stress response. *RNA*. 2018;24(6):841-52.
- 442 3. Abbink TEM, Wisse LE, Jaku E, Thiecke MJ, Voltolini-González D, Fritsen H, et al.
443 Vanishing white matter: deregulated integrated stress response as therapy target. *Annals of
444 clinical and translational neurology*. 2019;6(8):1407-22.
- 445 4. Sidrauski C, Tsai JC, Kampmann M, Hearn BR, Vedantham P, Jaishankar P, et al.
446 Pharmacological dimerization and activation of the exchange factor eIF2B antagonizes the
447 integrated stress response. *elife*. 2015;4:e07314.
- 448 5. Brush MH, Shenolikar S. Control of cellular GADD34 levels by the 26S proteasome.
449 *Molecular cellular biology*. 2008;28(23):6989-7000.
- 450 6. Dooves S, Bugiani M, Postma NL, Polder E, Land N, Horan ST, et al. Astrocytes are
451 central in the pathomechanisms of vanishing white matter. *The Journal of Clinical
452 Investigation*. 2016;126(4):1512-24.
- 453 7. Leferink PS, Dooves S, Hillen AEJ, Watanabe K, Jacobs G, Gasparotto L, et al.
454 Astrocyte Subtype Vulnerability in Stem Cell Models of Vanishing White Matter. *Annals of
455 Neurology*. 2019;86(5):780-92.
- 456 8. Zhou L, Li P, Chen N, Dai L-F, Gao K, Liu Y-N, et al. Modeling vanishing white matter
457 disease with patient-derived induced pluripotent stem cells reveals astrocytic dysfunction. *CNS
458 Neuroscience & Therapeutics*. 2019;25(6):759-71.
- 459 9. Atzmon A, Herrero M, Sharef-Eshed R, Gilad Y, Senderowitz H, Elroy-Stein O. Drug
460 screening identifies sigma-1-receptor as a target for the therapy of VWM leukodystrophy.
461 *Frontiers in molecular neuroscience*. 2018;11:336.
- 462 10. Wong YL, LeBon L, Basso AM, Kohlhaas KL, Nikkel AL, Robb HM, et al. eIF2B
463 activator prevents neurological defects caused by a chronic integrated stress response. *ELife*.
464 2019;8:e42940.
- 465 11. Weng T-Y, Tsai S-YA, Su T-P. Roles of sigma-1 receptors on mitochondrial functions
466 relevant to neurodegenerative diseases. *Journal of biomedical science*. 2017;24(1):74.

467 12. Park WH, Kim SH. MG132, a proteasome inhibitor, induces human pulmonary
468 fibroblast cell death via increasing ROS levels and GSH depletion. *J Oncology reports.*
469 2012;27(4):1284-91.

470 13. Jiang H-Y, Wek RC. Phosphorylation of the α -subunit of the eukaryotic initiation
471 factor-2 (eIF2 α) reduces protein synthesis and enhances apoptosis in response to proteasome
472 inhibition. *Journal of Biological Chemistry.* 2005;280(14):14189-202.

473 14. Brush MH, Weiser DC, Shenolikar S. Growth arrest and DNA damage-inducible
474 protein GADD34 targets protein phosphatase 1 alpha to the endoplasmic reticulum and
475 promotes dephosphorylation of the alpha subunit of eukaryotic translation initiation factor 2.
476 *Molecular and cellular biology.* 2003;23(4):1292-303.

477 15. Teske BF, Fusakio ME, Zhou D, Shan J, McClintick JN, Kilberg MS, et al. CHOP
478 induces activating transcription factor 5 (ATF5) to trigger apoptosis in response to
479 perturbations in protein homeostasis. *Mol Biol Cell.* 2013;24(15):2477-90.

480 16. Garcia-Segura LM. Hormones and brain plasticity: Oxford University Press; 2009.

481 17. Turón-Viñas E, Pineda M, Cusí V, López-Laso E, Del Pozo RL, Gutiérrez-Solana LG,
482 et al. Vanishing white matter disease in a spanish population. *Journal of central nervous system
483 disease.* 2014;6:JCNSD. S13540.

484 18. Petnikota H, Madhuri V, Gangadharan S, Agarwal I, Antonisamy B. Retrospective
485 cohort study comparing the efficacy of prednisolone and deflazacort in children with muscular
486 dystrophy: A 6 years' experience in a South Indian teaching hospital. *Indian J Orthop.*
487 2016;50(5):551-7.

488 19. McAdam LC, Mayo AL, Alman BA, Biggar WD. The Canadian experience with long-
489 term deflazacort treatment in Duchenne muscular dystrophy. *Acta Myol.* 2012;31(1):16-20.

490 20. Kawasaki T, Kitao T, Nakagawa K, Fujisaki H, Takegawa Y, Koda K, et al. Nitric
491 oxide-induced apoptosis in cultured rat astrocytes: Protection by edaravone, a radical
492 scavenger. *Glia.* 2007;55(13):1325-33.

493 21. Sato T, Mizuno K, Ishii F. A novel administration route of edaravone-II: mucosal
494 absorption of edaravone from edaravone/hydroxypropyl-beta-cyclodextrin complex solution
495 including L-cysteine and sodium hydrogen sulfite. *Pharmacology.* 2010;85(2):88-94.

496 22. Parikh A, Kathawala K, Tan CC, Garg S, Zhou X-F. Development of a novel oral
497 delivery system of edaravone for enhancing bioavailability. *International journal of
498 pharmaceuticals.* 2016;515(1-2):490-500.

499 23. Rothstein JD. Edaravone: a new drug approved for ALS. *Cell.* 2017;171(4):725.

500 24. Wu Y, Pan Y, Du L, Wang J, Gu Q, Gao Z, et al. Identification of novel EIF2B
501 mutations in Chinese patients with vanishing white matter disease. *Journal of human genetics.*
502 2009;54(2):74-7.

503 25. Ortori C, Barrett D, Fischer P, Halliday M, Radford H, Sekine Y, et al. Partial
504 restoration of protein synthesis rates by the small molecule ISRIB prevents neurodegeneration
505 without pancreatic toxicity. 2015.

506 26. Sidrauski C, Acosta-Alvear D, Khoutorsky A, Vedantham P, Hearn BR, Li H, et al.
507 Pharmacological brake-release of mRNA translation enhances cognitive memory. *Elife.*
508 2013;2:e00498.

509 27. Palam L, Gore J, Craven K, Wilson J, Korc M. Integrated stress response is critical for
510 gemcitabine resistance in pancreatic ductal adenocarcinoma. *Cell death & disease.*
511 2015;6(10):e1913-e.

512 28. Nguyen HG, Conn CS, Kye Y, Xue L, Forester CM, Cowan JE, et al. Development of
513 a stress response therapy targeting aggressive prostate cancer. *Science translational medicine.*
514 2018;10(439):eaar2036.

515 29. Wang L, Popko B, Tixier E, Roos RP. Guanabenz, which enhances the unfolded protein
516 response, ameliorates mutant SOD1-induced amyotrophic lateral sclerosis. *Neurobiology of*
517 *disease*. 2014;71:317-24.

518 30. Halliday M, Radford H, Sekine Y, Moreno J, Verity N, Le Quesne J, et al. Partial
519 restoration of protein synthesis rates by the small molecule ISRIB prevents neurodegeneration
520 without pancreatic toxicity. *Cell death & disease*. 2015;6(3):e1672-e.

521 31. Wong YL, LeBon L, Edalji R, Lim HB, Sun C, Sidrauski C. The small molecule ISRIB
522 rescues the stability and activity of Vanishing White Matter Disease eIF2B mutant complexes.
523 *Elife*. 2018;7:e32733.

524 32. Vuddanda PR, Chakraborty S, Singh S. Berberine: a potential phytochemical with
525 multispectrum therapeutic activities. *Expert opinion on investigational drugs*.
526 2010;19(10):1297-307.

527 33. Yu W, Sheng M, Xu R, Yu J, Cui K, Tong J, et al. Berberine protects human renal
528 proximal tubular cells from hypoxia/reoxygenation injury via inhibiting endoplasmic reticulum
529 and mitochondrial stress pathways. *Journal of translational medicine*. 2013;11(1):24.

530 34. Li Z, Geng Y-N, Jiang J-D, Kong W-J. Antioxidant and anti-inflammatory activities of
531 berberine in the treatment of diabetes mellitus. *Evidence-Based Complementary Alternative*
532 *Medicine*. 2014;2014.

533 35. Raini G, Sharet R, Herrero M, Atzmon A, Shenoy A, Geiger T, et al. Mutant eIF2B
534 leads to impaired mitochondrial oxidative phosphorylation in vanishing white matter disease.
535 2017;141(5):694-707.

536 36. Guiraud S, Davies KE. Pharmacological advances for treatment in Duchenne muscular
537 dystrophy. *Current opinion in pharmacology*. 2017;34:36-48.

538 37. Liu Y, Wang W, Li Y, Xiao Y, Cheng J, Jia J. The 5-lipoxygenase inhibitor zileuton
539 confers neuroprotection against glutamate oxidative damage by inhibiting ferroptosis.
540 *Biological Pharmaceutical Bulletin*. 2015;38(8):1234-9.

541 38. Parry GJ, Rodrigues CM, Aranha MM, Hilbert SJ, Davey C, Kelkar P, et al. Safety,
542 tolerability, and cerebrospinal fluid penetration of ursodeoxycholic acid in patients with
543 amyotrophic lateral sclerosis. *Journal of Clinical Neuropharmacology*. 2010;33(1):17-21.

544 39. Boatright JH, Nickerson JM, Moring AG, Pardue MT. Bile acids in treatment of ocular
545 disease. *Journal of ocular biology*. 2009;2(3):149.

546 40. Foster SL, Kendall C, Lindsay AK, Ziesel AC, Allen RS, Mosley SS, et al. Development of Bile Acids as Anti-Apoptotic and Neuroprotective Agents in Treatment of
547 Ocular Disease. *Drug Product Development for the Back of the Eye*: Springer; 2011. p. 565-
549 76.

550 41. Barros SR, Parreira SC, Miranda AF, Pereira AM, Campos NM. New insights in
551 vanishing white matter disease: Isolated bilateral optic neuropathy in adult onset disease.
552 *Journal of Neuro-Ophthalmology*. 2018;38(1):42-6.

553 42. Bell SM, Barnes K, Clemmens H, Al-Rafiah AR, Al-ofi EA, Leech V, et al. Ursodeoxycholic acid improves mitochondrial function and redistributes Drp1 in fibroblasts
554 from patients with either sporadic or familial Alzheimer's disease. *Journal of molecular*
555 *biology*. 2018;430(21):3942-53.

556 43. Denham M, Dottori M. Neural differentiation of induced pluripotent stem cells.
557 *Neurodegeneration*: Springer; 2011. p. 99-110.

558 44. Vichai V, Kirtikara K. Sulforhodamine B colorimetric assay for cytotoxicity screening.
559 *Nature protocols*. 2006;1(3):1112.